Supplementary Materials

Fast parameter optimization for high-fidelity crystal plasticity simulation using active learning

Meirong Jiang[1], Xiaobing Hu[2,*], Chen Xing[1], Zhongsheng Yang[1], Yiming Chen[1], Junjie Li[1], Zhijun Wang[1], Jincheng Wang[1,*]

[1]State Key Laboratory of Solidification Processing, Northwestern Polytechnical University, Xi'an 710072, Shaanxi, China.
[2]Xi'an Rare Metal Materials Institute Co. Ltd, Xi'an 710016, Shaanxi, China.

[*]**Correspondence to:** Prof. Jincheng Wang, State Key Laboratory of Solidification Processing, Northwestern Polytechnical University, Youyi campus, 127 West Youyi Road, Beilin District, Xi'an 710072, Shaanxi, China. E-mail: jchwang@nwpu.edu.cn; Dr. Xiaobing Hu, Xi'an Rare Metal Materials Institute Co. Ltd, No. 996, Tiangu Qi Road, High-Tech Zone, Xi'an 710016, Shaanxi, China. E-mail: xbhu5022@163.com

1. Hyperparameters for SVR, RF and GPR models.

Figure S1 exhibits the accuracy changes of random forest (RF), support vector regression (SVR) and GPR models with different combination conditions of hyperparameters. From Supplemenrary Figure 1(a), it can be observed that the highest prediction accuracy was obtained when the RBF kernel's length related coefficient γ is 1.45 and the regularization coefficient C is 45, as shown by the yellow dot in the figure. From Supplemenrary Figure 1(b), it can observed that the highest prediction accuracy of the RF was achieved with the number of trees N of 95 and the maximum tree depth H of 7, as shown by the yellow dot in the figure. From Supplemenrary Figure 1(c), when the scale parameter $Length\_scale$ is 1.85, the prediction accuracy of the GPR model is highest.

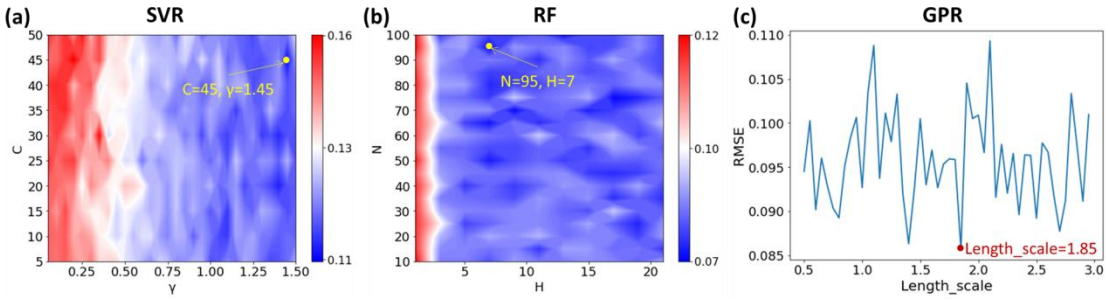

Supplementary Figure 1. RMSE changes of the three models with different combinations of hyperparameters. (a) SVR. (b) RF. (c) GPR. Here, both SVR and GPR employ a Gaussian kernel (or named Radial Basis Function kernel).

2. An initial training set

The initial 26 groups of crystal plasticity parameter combinations by selected randomly for Al-Cu eutectic materials were displayed in Supplemenrary Table 1.

Supplementary Table 1 Presetting 26 groups of $\dot{\gamma}_{0\_Al}$, $\dot{\gamma}_{0\_Al_2Cu}$ and H_{Al} parameter combination of $\dot{\gamma}_{0\_Al}$, $\dot{\gamma}_{0\_Al_2Cu}$ and H_{Al}

Numbers	Parameters			
	$\dot{\gamma}_{0\_Al}$	$\dot{\gamma}_{0\_Al_2Cu}$	H_{Al} (MPa)	H_{Al_2Cu} (MPa)
①	1.0×10^{-2}	1.0×10^{-3}	10	100
②	1.0×10^{-2}	2.0×10^{-2}	10	20
③	1.0×10^{-2}	1.0×10^{-5}	10	100
④	1.0×10^{-2}	1.0×10^{-5}	10	1000
⑤	5.0×10^{-4}	1.0×10^{-5}	900	1000
⑥	5.0×10^{-4}	1.0×10^{-5}	500	600
⑦	1.0×10^{-2}	1.0×10^{-3}	500	600
⑧	3.0×10^{-3}	5.0×10^{-4}	10	100
⑨	3.0×10^{-3}	5.0×10^{-4}	100	150
⑩	5.0×10^{-3}	1.0×10^{-4}	500	600
⑪	5.0×10^{-3}	1.0×10^{-4}	500	600
⑫	5.0×10^{-3}	1.0×10^{-5}	500	600
⑬	5.0×10^{-3}	5.0×10^{-5}	500	600
⑭	1.0×10^{-4}	1.0×10^{-5}	500	600
⑮	5.0×10^{-4}	1.0×10^{-5}	500	600
⑯	5.0×10^{-3}	5.0×10^{-4}	600	800
⑰	5.0×10^{-2}	5.0×10^{-3}	700	800
⑱	5.0×10^{-5}	1.0×10^{-5}	300	400
⑲	2.0×10^{-4}	5.0×10^{-4}	600	700
⑳	5.0×10^{-3}	5.0×10^{-4}	300	400
㉑	6.0×10^{-3}	3.0×10^{-3}	800	300
㉒	8.0×10^{-3}	4.0×10^{-3}	10	600
㉓	8.0×10^{-3}	3.0×10^{-4}	300	100
㉔	7.0×10^{-3}	3.0×10^{-4}	700	600
㉕	7.0×10^{-3}	3.5×10^{-4}	400	900
㉖	6.5×10^{-4}	3.5×10^{-4}	650	750

3. The CP simulated results of the xy shear deformation

Supplemenrary Figure 2 illustrates the engineering stress-strain curve for the Al-Cu eutectic material under *xy* shear deformation by the CP modeling, along with the motion of all potential slip systems within the aluminum phase. It can be observed that from Supplemenrary Figure 2(a), the stress in the α-Al phase is smaller than that in the θ-Al_2Cu phase, and the θ-Al_2Cu phase obviously does not experience plastic deformation. From Supplemenrary Figure 2(b), it can be found that the slip systems of $(\bar{1}11)[011]$, $(\bar{1}11)[101]$ and $(111)[0\bar{1}1]$ are activated, indicating that the deformation behavior in the α-Al phase mainly controlled by these active slip systems. Our conclusion is in good agreement with the experiment[1–3], demonstrating the reliability of the CP modeling.

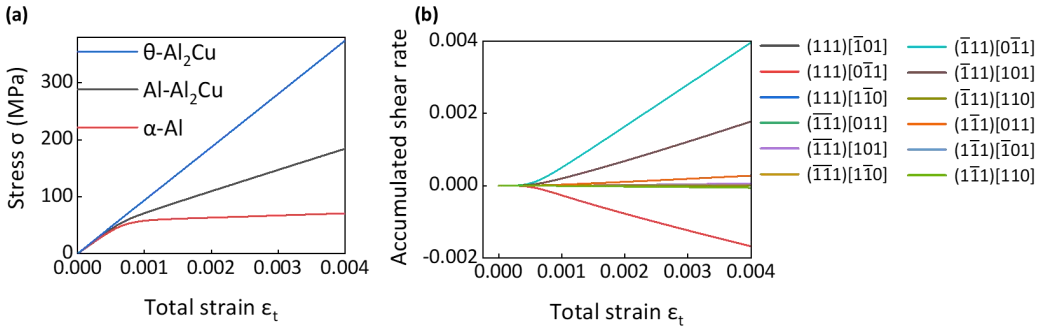

Supplementary Figure 2. Deformation behaviors at room temperature when the specimen of the Al-Cu eutectic alloy was sheared along the xy direction based on the CP simulation. (a) The engineering stress-strain curve. (b) Accumulated shear rate of all possible slip systems in α-Al phase for the Al-Cu eutectic alloy.

4. Mechanical response of Al-Cu eutectic alloy at 450℃

Supplemenrary Figure 3(a) depicts the engineering stress-strain curve for the Al-Cu eutectic alloy at 450 ℃. From the figure, it can be observed that the θ-Al_2Cu phase maintains a stress-strain curve that is perpetually above the Al-Cu eutectic, and the eutectic material's curve consistently surpasses that of the α-Al phase. This observation suggests that the stress-strain behavior of the Al-Cu eutectic material is a result of the combined effects of the α-Al and θ-Al_2Cu phases. Supplemenrary Figure 3(a) depicts the evolution of plastic strain with the increase of the total strain for the Al-Cu eutectic alloy at 450 ℃. It is evident that the α-Al phase exhibits a non-zero plastic strain ε_p at a total strain ε_t ($\varepsilon_t > \sim 0.0002$) that is considerably lower than the threshold for the θ-Al_2Cu phase ($\varepsilon_t > \sim 0.01$). This observation indicates that the α-Al phase initiates plastic deformation at an earlier stage compared to the θ-Al_2Cu phase. Nonetheless, after the onset of plastic deformation in the θ-Al_2Cu phase (when ε_p becomes non-zero), the difference in plastic strain between the θ-Al_2Cu and α-Al phases narrows with the increasing total strain ε_t. This implies that while the θ-Al_2Cu phase is less prone to plastic deformation, it experiences a swift and significant rise in plastic strain ε_p once deformation is initiated.

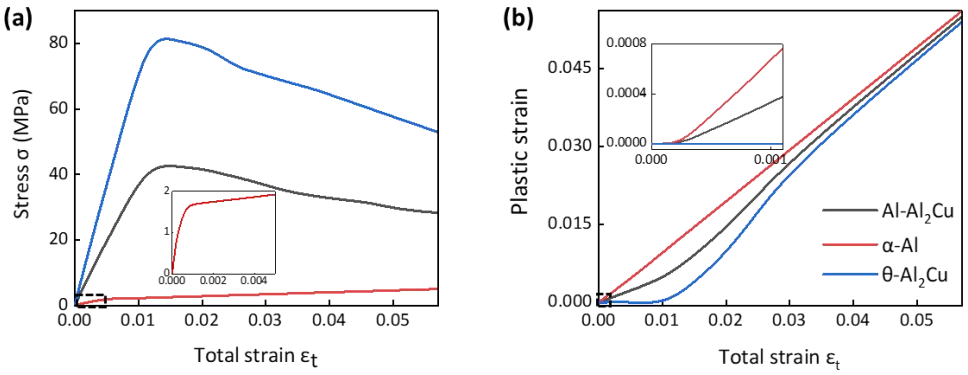

Supplementary Figure 3. Mechanical response of Al-Cu eutectic alloy at 450 ℃ based on the crystal plasticity simulation. (a) Engineering stress-strain curves for Al-Cu eutectic alloy, α-Al and θ-Al_2Cu. (b) Plastic strain variations with the total strain for Al-Cu eutectic alloy, α-Al and θ-Al_2Cu.

5. Engineering stress-strain for Al-Cu eutectic alloy at different temperatures

Supplemenrary Figure 4 displays a comparison of experimental and simulated stress-strain curves for the Al-Cu eutectic alloy at different temperatures. The simulated stress-strain curves are derived from the optimal CP parameters identified through the AL parameter selection strategy proposed in this study, as shown in Supplemenrary Table 2. The details of the CP model present the literature[4–6]. From Supplemenrary Figure 4, it can be observed that the CP stress-strain curve (black curve) is in good agreement with the experiment (red curve), demonstrating the reliability of the optimal CP parameters. This also illustrated the effectiveness of the parameter search strategy proposed in this study for CP parameter optimization.

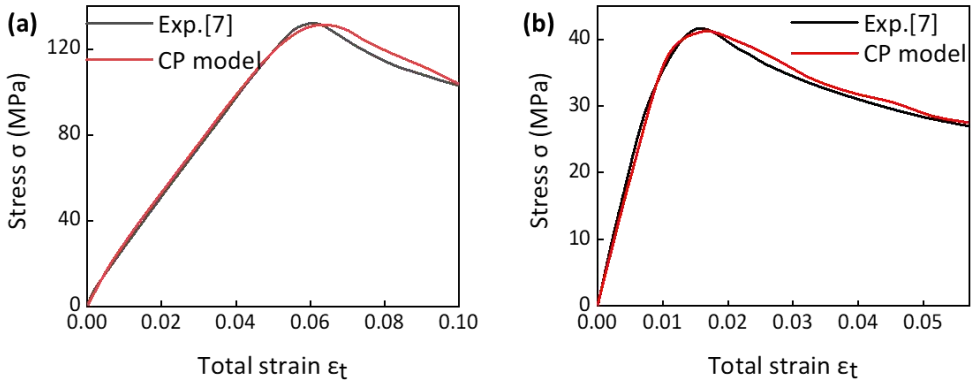

Supplementary Figure 4. Comparison of the engineering stress-strain curve between the CP simulation and the experiment[7] for the Al-Cu eutectic alloy at different temperatures. (a) 325 ℃. (b) 450 ℃.

Supplementary Table 2. The optimal CP parameters for the Al-Cu eutectic alloy at high temperatures based on the search strategy proposed in this study.

Parameter	Value	Parameter	Value
K_{Sw}=K_{Se}	0.015	$\rho^{\theta}_{Sw,0}$=$\rho^{\theta}_{Se,0}$ (m^{-2})	1.0×10^{13}
υ	0.5	C_{Sw}=C_{Se}	0.5
d_{Sw}=d_{Se} (nm)	5.0	$h^{\alpha\theta}$	0.1

References

1. Maddin R. LXXXIII. Quench hardening in aluminium single crystals. Physical Metallurgy 1955;46(7):735–743; doi: 10.1080/14786440708520600.

2. Davidson CJ, Chadwick GA. Effect of heat treatment and interlamellar spacing on the tensile deformation of the aligned Al-$CuAl_2$ eutectic. Acta Metall 1980;28(1):61–73; doi: 10.1016/0001-6160(80)90041-3.

3. Jabczynski FSJ, Cantor B. The solidification and mechanical properties of chill-cast Al-Al_3Ni and Al-Al_2Cu eutectic alloys. J Mater Sci 1981;16:2269–2280; doi: 10.1007/BF00542390.

4. Jiang M, Chen Y, Yang Z, et al. Crystal plasticity modeling of deformation behavior of Al–Al_2Cu eutectics based on high-fidelity representative microstructures. J Mater Res Technol 2024;29:5259–5270; doi: 10.1016/j.jmrt.2024.02.204.

5. Zhao J, Lv L, Wang K, et al. Effects of strain state and slip mode on the texture evolution of a near-α TA15 titanium alloy during hot deformation based on crystal plasticity method. J Mater Sci Technol 2020;38:125–134; doi: 10.1016/j.jmst.2019.07.051.

6. Zhao J, Lv L, Liu G, et al. Analysis of deformation inhomogeneity and slip mode of TA15 titanium alloy sheets during the hot tensile process based on crystal plasticity model. Mat Sci Eng A 2017;707:30–39; doi: 10.1016/j.msea.2017.08.094.

7. Hong JH, Hong JH. Tensile properties of unidirectionally solidified Al−$CuAl_2$ eutectic composite. Journal of Korea Foundry Society 1990;10(6):503–508.